# Electrochemical and corrosion characterisation of magnetron sputtered Fe–Cr–Ni–Ta alloy

**Konstantinas Leinartas, Meilutė Samulevičienė, Audrius Bagdonas, Aloyzas Sudavičius, and Eimutis Juzeliūnas**

*Institute of Chemistry,*
*A. Goštauto 9,*
*LT-2600 Vilnius, Lithuania*

Corrosion and electrochemical behaviour of magnetron sputtered alloy Fe–Cr–Ni–Ta was studied by quartz crystal microbalance (EQCM), electrochemical impedance spectroscopy (EIS), dc-voltammetry and X-ray photoelectron spectroscopy (XPS). The alloys were deposited on quartz substrates by means of DC magnetron sputtering, using targets from an AISI 316 stainless steel and pure tantalum. The content of elements in the deposit was determined by XPS analysis. Corrosion and electrochemical behaviour of the alloy was studied in 5% NaCl (pH 5.75), 5% NaCl + HCl (pH 3.3) and 10 M HCl. The corrosion resistance of Fe–Cr–Ni–Ta was superior to that of AISI 316 stainless steel. This was evident from measurements of the zero current potential, the anodic currents and the breakdown potentials. The tantalum-inhibiting effect in acid medium was significantly higher than in neutral one. Thus, the anodic activity of Fe–Cr–Ni–Ta in 5% NaCl was about three times lower than the activity of AISI-316, whereas in 10 M HCl the difference was of about three orders of magnitude. The EQCM experiments revealed that the sputtered alloy actively dissolved during the first immersion stages (*ca*. 10 min) in 10 M HCl, and with immersion time the surface became passive. The XPS analysis showed that during corrosion the passive film was enriched by tantalum, which caused the corrosion inhibition.

**Key words**: magnetron sputtered alloys, stainless steel, tantalum, corrosion, EQCM

## INTRODUCTION

Sputtered alloys, due to their chemical homogeneity and amorphous properties, normally have superior anticorrosive properties when compared to conventional crystalline alloys. The sputtered alloys are free of crystallographic defects (dislocations, crystal imperfections, distortions, grain boundaries, second phase elements, etc.), and therefore the passive films on these alloys are more uniform and contain less weak sites than films on crystalline surfaces. That is why sputter deposition has attracted considerable attention in the recent years as an effective tool to deposit corrosion-resistant coatings [1–21].

The sputtering procedure makes it possible to create alloy compositions with the metals whose melting point is higher than the boiling point of other alloy components. Examples are a successful sputter codeposition of Ta with Cr and Fe–Cr–Ni [20, 21]. It has been shown that Fe–Cr–Ni–Ta alloys have an extremely high corrosion resistance in 12 M HCl [21]. The corrosion rates of the alloy were found to be more than six orders of magnitude lower than those of tantalum-free stainless steel. Such a high corrosion resistance was explained in terms of the formation of the double oxyhydroxide film containing chromium and tantalum cations.

In this paper we report corrosion behaviour of sputter-deposited Fe–Cr–Ni–Ta alloy in solutions at different pH. The experiments were performed in almost neutral (pH 5.75), slightly acid (pH 3.3) and strongly acid (10 M HCl) media. The alloy was deposited by DC magnetron sputtering technique on quartz discs, which in conjunction with a nanobalance apparatus served as a sensitive corrosion detector enabling to register corrosion dynamics with nanogram resolution.

## EXPERIMENTAL

The target for magnetron sputtering was made of commercially available AISI 316 stainless steel (exact composition is given in Table) and pure tantalum (99.95). The stainless steel target was a disc 30 mm in diameter and 0.5 mm thick. A rectangular gap ($4 \times 2.5$ mm) was cut off in the stainless steel target

Table. **Content (in weight %) of elements of the sputter-deposited Fe–Cr–Ni–Ta alloy on quartz, using as a target AISI 316 stainless steel and tantalum. The samples were analysed by XPS after surface etching by ionised argon within 1 min, which corresponded to *ca*. 10 nm depth**

| AISI 316 | | | | | | | | |
|---|---|---|---|---|---|---|---|---|
| Fe | Cr | Ni | Mn | Mo | Si | Cu | Ta | O |
| 68.3 | 20.1 | 9.4 | 1.3 | 0.22 | 0.23 | 0.35 | – | – |
| Sputtered deposit | | | | | | | | |
| 42.9 | 9.2 | 5.7 | 0.45 | 1.37 | – | – | 37.4 | 3.1 |

and a tantalum plate of the same dimensions was mounted in the gap. The vacuum in the MS chamber was maintained at $1.33 \times 10^{-4}$ Pa. The working gas was Ar and its pressure was maintained at 0.1–0.2 Pa. The temperature in the chamber was *ca.* 100 °C. The Ar ionisation current was 60 mA and the voltage was 600 V. The sputtering duration was 6–8 min, which corresponded to a coating thickness of *ca*. 0.2 μm. More details about the MS apparatus and procedure used are given elsewhere [17–19].

The coating composition was analysed by X-ray photoelectron spectroscopy (XPS), using surface etching by ionised argon. The spectra were recorded by an ESCALAB MKII spectrometer (Great Britain), using X-radiation of $MgK_\alpha$ (1253.6 eV, pass energy 20 eV). The samples were etched in the preparation chamber by ionised argon in a vacuum of $5 \times 10^{-4}$ Pa. An accelerating voltage of *ca*. 5 kV and a beam a current of 100 μA/cm$^2$ were used. The etching was performed at current of 100 μA, which corresponded to an etching rate of *ca*. 10 nm/min. The data on binding energies ($E_b$) were used from [22, 23]. The sputtered coatings contained about 40% in mass of Ta (Table).

The EQCM experimental device was analogous to that described previously [24]. Quartz discs 15 mm in diameter (AT plane) with the fundamental frequency $f_0$ = 5 MHz were used (KVG Quartz Crystal Technology GmbH, Germany). Both sides of the discs were coated by the alloy, using a magnetron-sputtering technique. The coated discs were mounted in a special window of an electrochemical cell, with one side exposed to the cell compartment.

The stainless steel electrodes were cut in the form of discs with a diameter of 15 mm and a thickness of 0.5 mm from an AISI 316 plate. Its surface was polished by an abrasive SiC paper (grade 1000), rinsed with alcohol and water and dried under ambient conditions. The specimen then was pressed via a "Vitron" o-ring to the window of the electrochemical cell.

A saturated Ag/AgCl electrode was used as the reference electrode and a platinum foil served as a counter-electrode. Impedance spectroscopy as well as voltammetric measurements have been conducted by an IM6 apparatus from Zahner (Germany).

## RESULTS AND DISCUSSION

Figure 1 shows the voltammetric behaviour of AISI 316 stainless steel (curve 1) and the sputtered Fe–Cr–Ni–Ta alloy (curve 2) in 5% NaCl solution (pH 5.75). The zero current potential of the sputtered specimen is *ca*. 200 mV greater than that of stainless steel, which implies a higher passivity of the sputtered specimen. The anodic curves indicated a rather large passive region (E = –0.2 ÷ –0.3 V), in which anodic limiting currents differed negligibly for both specimens. The values of the breakdown potential (*i.e*. the potential at which the passive layer begins to destroy) are also close for both specimens (*ca*. 0.35 V); however, above this potential the bulk

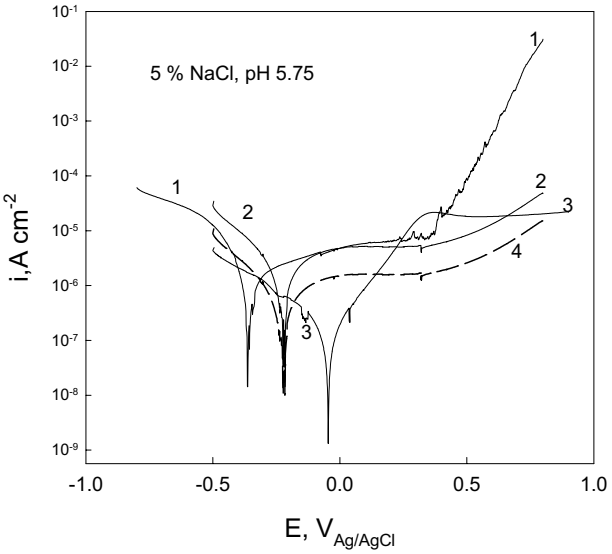


Fig. 1. Voltammetric characteristics for AISI 316 (1), magnetron-sputtered Fe–Cr–Ni–Ta (2) and pure tantalum (3) obtained at v = 5 mV s$^{-1}$ in 5% NaCl (pH 5.75) open to air. Curve 4 represents the result of curve 2 correction according to the ratio $K = C_{ss}/C_{sd}$ (for details, see Fig. 2)

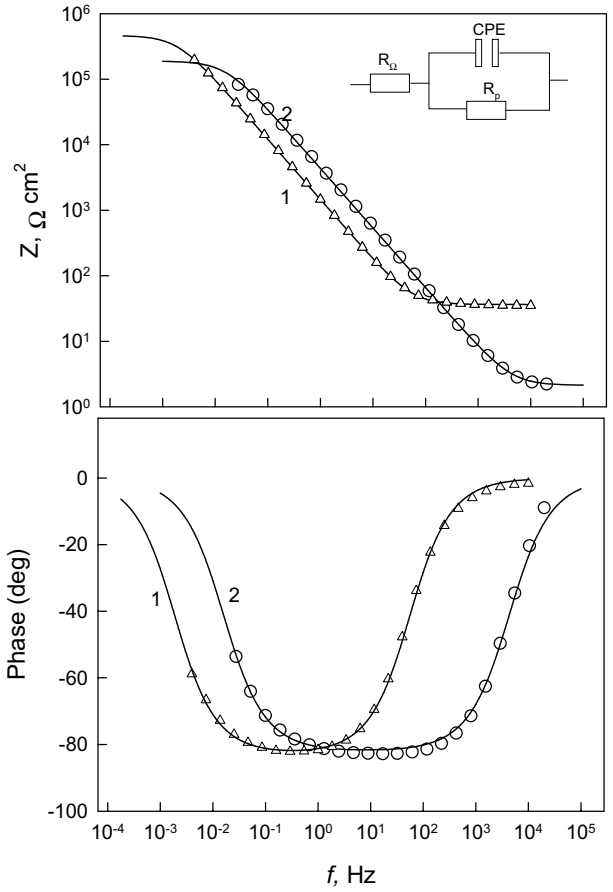


Fig. 2. Impedance diagram obtained at open circuit potential for magnetron-sputtered Fe–Cr–Ni–Ta alloy (1) and AISI 316 steel (2) in 5% NaCl solution open to air. Measurements were started after 1 h immersion in the solution. The symbols represent the experimental data, and the lines are fitting the results obtained assuming the equivalent circuit which consists of the solution resistance $R_\Omega$ and polarization resistance $R_p$ in parallel with the constant phase element (CPE). Fitting parameters for sputtered alloy (curve 1): $R_\Omega$ = 36 Ω cm², $R_p$ = 467 kΩ cm², $C_{sd}$ = 63 μF cm$^{-2}$ (n = 0.92). Fitting parameters for AISI 316 (curve 2): $R_\Omega$ = 2.1 Ω cm², $R_p$ = 209 kΩ cm², $C_{ss}$ = = 19.5 μF cm$^{-2}$ (n = 0.9)

stainless steel dissolves much faster than the sputtered alloy.

The electrochemical impedance spectra obtained under open circuit conditions for both Fe–Cr–Ni–Ta alloy and AISI 316 stainless steel are shown as Bode plots in Fig. 2. The corrosion resistance is usually reflected by the polarisation resistance ($R_p$), which yields the low-frequency domain, in which impedance does not actually depend upon the frequency and the phase angle is close to 0°. However, due to the high corrosion resistance of the specimens such a domain could not be determined within a practical frequency range. The $R_p$ value could be approximately estimated by a fitting procedure assuming an appropriate equivalent circuit. The experimental data in Fig. 2 (symbols) were well fitted (lines) assuming an equivalent circuit, which consisted of solution resistance ($R_\omega$) and $R_p$ in parallel with the constant phase element (CPE) whose impedance is given by $Z_{CPE} = 1/C(j\omega)^{-n}$. The constant-phase element usually is used instead of the ideal capacity in order to take into account the capacitance of the space charge within the passive film.

The polarisation resistance of the sputtered alloy was found from the fitting procedure to be more than twice higher than the resistance of AISI 316 ($R_p$ = 467 kΩ cm² and $R_p$ = 209 kΩ cm², respectively). This implies that the Fe–Cr–Ni–Ta alloy corrosion resistance is higher than that of stainless steel.

The double layer capacity of the sputtered deposit was also higher than the capacity of stainless steel ($C_{sd}$ = 63 μF cm$^{-2}$ and $C_{ss}$ = 19.5 μF cm$^{-2}$, respectively). Such a difference is distinctive for sputtered and polished surfaces, as it was demonstrated previously when studying sputtered Au–Pd–In, Co–Cr–Mo and Ni–Cr–Mo alloys [19, 25]. This is quite understandable when taking into account that the actual area of the sputtered surface should be greater than the area of the mechanically polished surface, what is clearly seen on the SEM microphotograps (Fig. 3).

The voltammetric curve for pure tantalum treated in the same way as stainless steel is also given for comparison in Fig. 1. The anodic curve has a clear Tafel region between 0.1 V and 0.35 V, and above this the electrode becomes passive. The value of the zero current potential and the currents close to it indicate that the tantalum specimen is more resistant to corrosion than the two other specimens.

The experiments performed in 5% NaCl solution revealed a similar electrochemical behaviour of both Fe–Cr–Ni–Ta alloy and AISI 316 stainless steel. Some indications showed that the sputtered specimen was more resistant to corrosion; however, quantitatively this difference was not great.

It is significant that according to the EIS data the actual area of the sputtered alloy was about

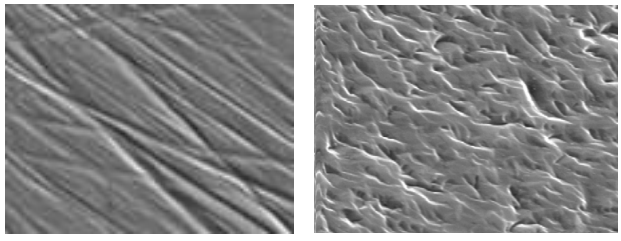

**a** **b**

Fig. 3. SEM micrographs of surface topography (×3000) of mechanically polished AISI 316 (*a*) and magnetron sputtered Fe–Cr–Ni–Ta alloy (*b*)

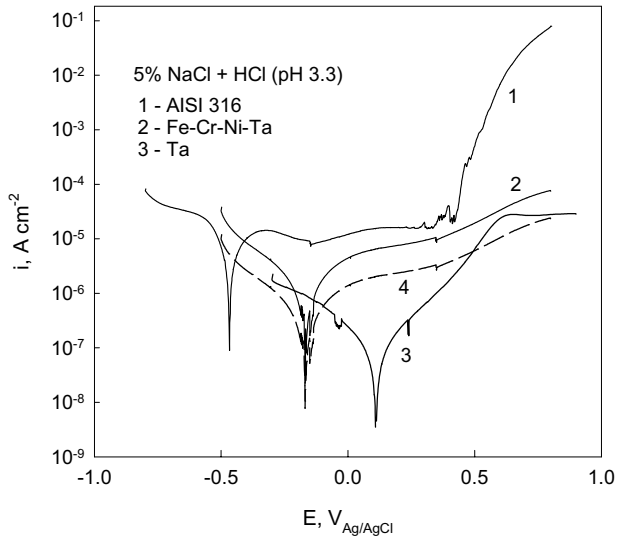


Fig. 4. Voltammetric characteristics for AISI 316 (1), magnetron-sputtered Fe–Cr–Ni–Ta (2) and pure tantalum (3) obtained at v = 5 mV $s^{-1}$ in 5% NaCl + HCl (pH 3.3) open to air. Curve 4 represents the result of curve 2 correction according to the ratio $K = C_{ss}/C_{sd}$ (for details, see Fig. 2)

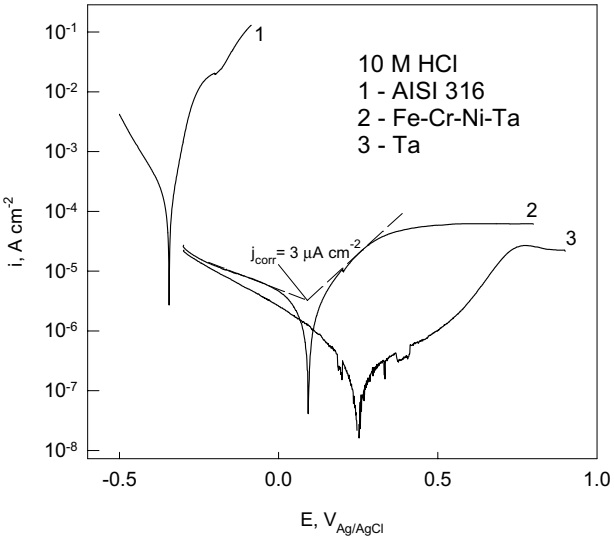


Fig. 5. Voltammetric characteristics for AISI 316 (1), magnetron-sputtered Fe–Cr–Ni–Ta (2) and pure tantalum (3) obtained at v = 5 mV $s^{-1}$ in 10 M HCl

three times larger than that of the stainless steel. Assuming the ratio $K = (C_{ss}/C_{sd})$ as a quantitative criterion of difference in actual areas, the curves in Fig. 1 can be adjusted relating them to the same actual area. After such a correction, the curve for sputtered alloy (curve 4, Fig. 1) is shifted down, what indicates that this specimen has a higher resistance as compared to AISI 316.

The voltammetric curves obtained in slightly acid NaCl solution (pH 3.3, Fig. 4) are qualitatively similar to those obtained in an almost neutral solution (pH 5.75, Fig. 1). However, the superior anticorrosive properties of Fe–Cr–Ni–Ta alloy in a slightly acidic medium are more pronounced, what is evident from the difference in the zero current potentials and the anodic limiting currents of both Fe–Cr–Ni–Ta and AISI 316. It is obvious from Fig. 4 that pure tantalum in an acidified solution is more resistant with respect to corrosion than the other two specimens.

A strong tantalum-inhibiting effect is observed in 10 M HCl, which represents a highly aggressive medium (Fig. 5). The zero current potential of the Fe–Cr–Ni–Ta alloy is about 0.5 V higher and the limiting anodic current is about two orders of magnitude lower than those observed for tantalum-free stainless steel. The voltammetric curve obtained for pure tantalum (curve 3, Fig. 5) indicates a significantly higher resistance to corrosion of this electrode as compared to the alloys.

Thus, the performed experiments clearly demonstrated that the tantalum inhibiting action in Fe–Cr–Ni–Ta alloy depends upon the solution acidity: the higher the acidity the more pronounced the inhibition effect. Only a slight corrosion inhibition was observed in almost neutral solution (pH 5.75, Fig. 1), the effect was more pronounced in slightly acid solution (pH 3.3, Fig. 4), and it was extremely great in 10 M HCl (Fig. 5).

To get a deeper insight into the corrosion behaviour of the sputtered alloy, the experiments using EQCM (Fig. 6) and XPS (Figs. 7 and 8) were performed. Quartz crystal microgravimetry was shown to be an effective approach for corrosive characte-

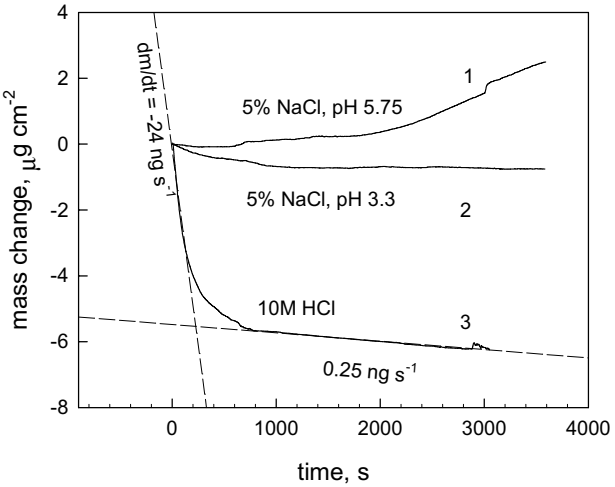


Fig. 6. Fe–Cr–Ni–Ta mass change determined by EQCM during corrosion in 5% NaCl (pH 5.75) (1), 5% NaCl + + HCl (pH 3.3) (2) and 10 M HCl (3) open to air

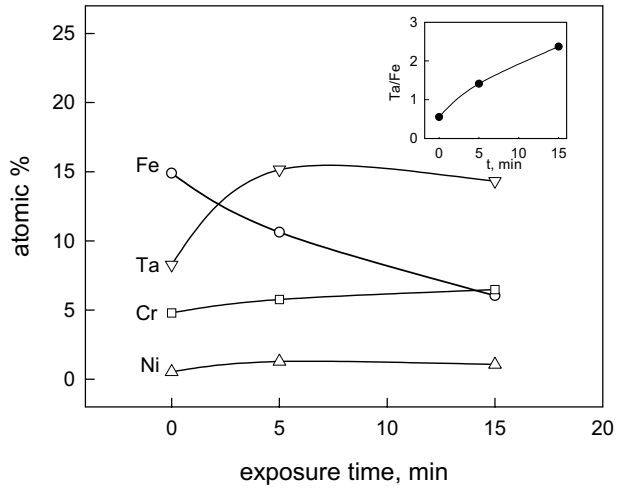


Fig. 7. Element concentrations (in atomic %) on Fe–Cr–Ni–Ta surface *vs*. immersion time in 10 M HCl obtained by XPS. Insertion shows an increase in the concentration ratio Ta/Fe as a function of sample exposure time to 10 M HCl

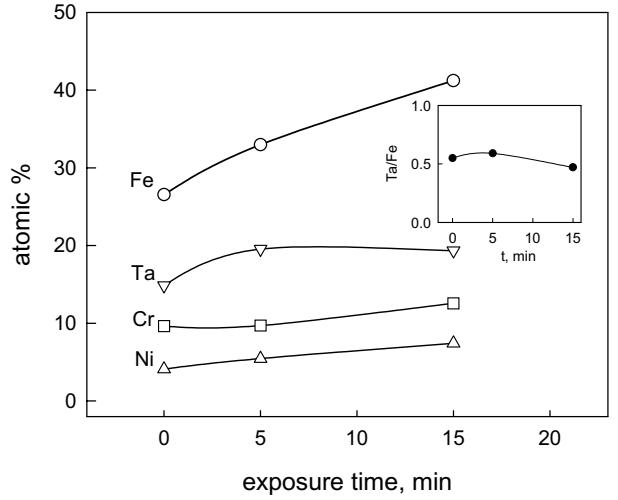


Fig. 8. Element concentrations (in atomic %) *vs*. immersion time in 10 M HCl obtained by XPS after surface sputtering by ionised argon, which corresponds to *ca*. 2 nm depth

risation of sputtered alloys in gaseous and liquid environments [17, 19, 25, 26]. The advantages of the method include the information continuity (*i.e.* the information availability at any practical time interval), nanogram resolution and possibility to combine the EQCM measurements with other methods (for instance, spectroscopy).

Figure 6 represents the data on mass change during Fe–Cr–Ni–Ta corrosion in solutions open to air at different pH. The distinctive mass growth after electrode immersion into an almost neutral solution (pH 5.75) implied the corrosion process with accumulation of scarcely soluble corrosion products on the alloy surface. A slight mass decrease is observed in acidified solution (pH 3.3), which indicates metal dissolution to be prevailing, although the possibility of accumulation of corrosion products on the surface could not be totally disclaimed. A fast alloy dissolution rate (dm/dt = –24 ng $s^{-1}$ $cm^{-2}$) is observed within the first stages of immersion (*ca*. 200 s) in 10 M HCl. The dissolution rate decays with the immersion time, and after *ca*. 10 min it becomes close to that observed in the slightly acid solution (curve 2). Thus, the "history" of active dissolution leads to a high alloy resistance against acid attack.

The corrosion rate from the EQCM results could also be expressed in electric units (A $cm^{-2}$), as it is a common practice in corrosion investigations using electrochemical methods. The ratio between the oscillation frequency change of quartz resonator and mass change during corrosion is given by [24, 27–29]:

$$j_{corr} = \pm (nFC/\Delta M)\ (df/dt), \qquad (1)$$

where $j_{corr}$ is the corrosion current density (A $cm^{-2}$), $df/dt$ is the rate of the change of quartz oscillation frequency, $F$ is the Faraday constant, $n$ is the number of electrons in the corrosion reaction, $\Delta M$ is the molar mass of the particles responsible for the mass gain (O, OH, OOH, etc.) or mass loss ($Me^{z+}$) during corrosion, and $C$ is the proportional coefficient between the frequency and mass change. According to the well-known Sauerbrey's equation [30], $C$ = = 18 ng $Hz^{-1}cm^{-2}$ when the main resonance frequency is $f_0$ = 5 MHz.

Assuming the mass change rate $dm/dt$ = 1 ng/s and the above $C$ value, we can simplify ratio (1) to

$$j_{corr} = 9.65 \times 10^{-5}\ (n/\Delta M). \qquad (2)$$

As has been shown previously, $j_{corr}$ calculations according to (1) give the same result for different oxides ($Me_2O$, MeO, $Me_2O_3$ $MeO_2$ and $MeO_3$) [25]. Thus, $j_{corr}$ calculation does not require to know what oxides and in which proportion are formed during corrosion, it is enough to know that the corrosion products are oxides. The ratio (1) was also verified for metal dissolution without formation of scarcely soluble compounds on electrode surface, as is the case for cadmium corrosion in acid media [28, 31].

We can assume that Fe, Cr and Ni are the main corroding components of the alloy under study (according to Figs. 1, 4 and 5, the zero current potentials of Ta electrode are significantly higher than those of the alloy). Iron, chromium and nickel have similar values of molar masses ($M_{Fe}$ = 56, $M_{Cr}$ = 52 and $M_{Ni}$ = 59) the average value of which equals

to the molar mass of iron. Assuming M = 56 and n = 2, we can calculate according to (1) that the initial mass decrease dm/dt = –24 ng $s^{-1}cm^{-2}$ in 10 M HCl (Fig. 6) yields the value $j_{corr}$ = 0.82 mA $cm^{-2}$. The constant mass decrease established after *ca*. 1000 seconds (dm/dt = –0.25 ng $s^{-1}cm^{-2}$) yields the corrosion current $j_{corr}$ = 0.85 μA $cm^{-2}$ for $n$ = = 2 and $j_{corr}$ = 1.27 μA $cm^{-2}$ for $n$ = 3, *i.e*. the values which are about three orders of magnitude lower than that calculated above for the initial stages. The corresponding value found from the extrapolation of the cathodic Tafel plot (Fig. 5) is $j_{corr} \approx$ $\approx 3$ μA $cm^{-2}$, which is comparable with the values derived from the EQCM information.

The XPS investigations showed that the concentration ratio of tantalum and iron (Ta/Fe) on the alloy surface tends to increase with immersion time in 10 M HCl (Fig. 7). So, prior to immersion, the concentration rate of both elements on the alloy surface is Ta/Fe ≈ 0.5, whereas it becomes about five times higher after a 15 min exposure to 10 M HCl (insertion in Fig. 7). However, such an increase was observed only on the specimen surface, *i.e.* in the passive layer, which on stainless steel grows only up to a few nanometers in thickness [32]. In deeper layers, however, the Ta/Fe concentration rate remains actually unaffected during corrosion, as is seen from analysis attained by using surface sputtering by ionised argon (*ca*. 2 nm depth, Fig. 8).

According to the results reported by Hashimoto et al., the passive film on Fe–Cr–Ni–Ta was composed mainly of double oxyhydroxides of chromium and tantalum, which were concluded to be responsible for the high resistance of the alloy to corrosion in hydrochloric acid solution [21]. The results reported in our paper showed that the degree of the resistance depends upon corrosion time. While after a certain time of immersion the alloy exhibits an extremely high corrosion resistance, in the first corrosion stages the corrosion rate can be rather high. As a result of the initial alloy susceptibility to corrosion, preferential iron dissolution takes place, what leads to enrichment of the passive layer by tantalum and, consequently, to the increased corrosion resistance.

## CONCLUSIONS

The Fe–Cr–Ni–Ta alloy was deposited on quartz substrates by using magnetron-sputtering technique and the targets from AISI 316 stainless steel and pure tantalum. The alloy formation by conventional melting is virtually impossible, because the melting point of tantalum is higher than the boiling points of other components.

The EIS and dc-voltammetry experiments revealed a superior anticorrosive resistance of Fe–Cr–Ni–Ta alloy to AISI-316 steel. The corrosion resistance of the alloy in 10 M HCl was about three orders of magnitude higher than that of AISI-316 steel. However, the analogous difference in 5% NaCl (pH 5.75) was only about three times. Thus, the inhibiting effect of tantalum was much more pronounced in acid media.

The EQCM experiments revealed that the sputtered alloy actively dissolved during the first corrosion stages, but the corrosion rate was significantly reduced with the corrosion time. The alloy dissolution was accompanied by enrichment of the passive layer with tantalum, which, in conjunction with other phenomena, caused the corrosion inhibition.

## ACKNOWLEDGEMENTS

The authors acknowledge Dr. V. Lisauskas for carrying out magnetron sputtering.

Received 6 December 2001
Accepted 3 January 2002

**References**

1. G. S. Frankel, R. C. Newman, C. V. Jahnes and M. A. Russak, *J. Electrochem. Soc.,* **140**, 2192 (1993).
2. H. Habazaki, K. Shimizu, P. Skeldon, G. E. Thompson and G. C. Wood. *Thin Solid Films,* **300**, 131 (1997).
3. H. Mitsui, H. Habazaki, K. Asami, K. Hashimoto and S. Mrowec, *Corros. Sci.,* **38**, 1431 (1996).
4. M. Mehmood, E. Akiyama, H. Habazaki, A. Kawashima, K. Asami and K. Hashimoto, *Corros. Sci.,* **41**, 1871 (1999).
5. M. Mehmood, E. Akiyama, H. Habazaki, A. Kawashima, K. Asami and K. Hashimoto, *Corros. Sci.,* **40**, 1 (1998).
6. M. Mehmood, E. Akiyama, H. Habazaki, A. Kawashima, K. Asami and K. Hashimoto, *Corros. Sci.,* **41**, 477 (1999).
7. P.-Y. Park, E. Akiyama, H. Habazaki, K. Asami and K. Hashimoto, *Corros. Sci.,* **37**, 1843 (1995).
8. P.-Y. Park, E. Akiyama, H. Habazaki, K. Asami, A. Kawashima and K. Hashimoto, *Corros. Sci.,* **38**, 1649 (1996).
9. P.-Y. Park, E. Akiyama, H. Habazaki, K. Asami, A. Kawashima and K. Hashimoto, *Corros. Sci.,* **38**, 1731 (1996).
10. P.-Y. Park, E. Akiyama, A. Kawashima, K. Asami and K. Hashimoto, *Corros. Sci.,* **38**, 397 (1996).
11. J. Bhattarai, E. Akiyama, H. Habazaki, A. Kawashima, K. Asami and K. Hashimoto, *Corros. Sci.,* **38**, 2071 (1995).
12. J. Bhattarai, E. Akiyama, H. Habazaki, A. Kawashima, K. Asami and K. Hashimoto, *Corros. Sci.,* **39**, 355 (1997).

13. J. Bhattarai, E. Akiyama, H. Habazaki, A. Kawashima, K. Asami and K. Hashimoto, *Corros. Sci.,* **40**, 19 (1998).
14. J. Bhattarai, E. Akiyama, H. Habazaki, A. Kawashima, K. Asami and K. Hashimoto, *Corros. Sci.,* **40**, 155 (1998).
15. J. H. Kim, E. Akiyama, H. Habazaki, A. Kawashima, K. Asami and K. Hashimoto, *Corros. Sci.,* **36**, 1817 (1994).
16. X.-Y. Li, E. Akiyama, H. Habazaki, A. Kawashima, K. Asami and K. Hashimoto, *Corros. Sci.,* **38**, 1269 (1996).
17. E. Juzeliūnas, K. Leinartas, M. Samulevičienė, D. Jelinskienė, A. Sudavičius, P. Miečinskas, V. Lisauskas and B. Vengalis. In: ICCE/7 (Seventh Annual International Conference on Composites Engineering), Denver, Colorado, USA, 405 (2000).
18. K. Leinartas, M. Samulevičienė, D. Jelinskienė, A. Sudavičius, V. Lisauskas, B. Vengalis and E. Juzeliūnas, *Chemija* 11/3, 117 (2000).
19. E. Juzeliūnas, K. Leinartas, M. Samulevičienė, P. Miečinskas, R. Juškėnas and A. Sudavičius, *Corros. Sci.* (Accepted).
20. J. H. Kim, E. Akiyama, H. Habazaki, A. Kawashima, K. Asami and K. Hashimoto, *Corros. Sci.,* **34**, 1947 (1993).
21. X.-Y. Li, E. Akiyama, H. Habazaki, A. Kawashima, K. Asami and K. Hashimoto, *Corros. Sci.,* **41**, 1849 (1999).
22. C. D. Wagner, W. M. Riggs, L. E. Davis, J. F. Moulder and G. E. Muilenberg, *Handbook of X-ray Photoelectron Spectroscopy*, Perkin Elmer Corporation, Minnesota (1978).
23. Practical Surface Analysis by Auger and X-ray Photoelectron Spectroscopy, Eds. D. Briggs and M. P. Seach, John Wiley and Sons (1983).
24. E. Juzeliūnas, P. Kalinauskas and P. Miečinskas, *J. Electrochem. Soc.,* **143**, 1525 (1996).
25. E. Juzeliūnas, K. Leinartas, M. Samulevičienė, A. Sudavičius, P. Miečinskas, R. Juškėnas, V. Lisauskas and B. Vengalis, *J. Solid State Electrochem*., On-line publication DOI 10 1007/s 100080100237.
26. K. Leinartas, P. Miečinskas, A. Sudavičius, D. Jelinskienė, R. Juškėnas, V. Lisauskas, B. Vengalis and E. Juzeliūnas. *J. Appl. Electrochem.,* **31(10)**, 1079 (2001).
27. M. Stratmann, W. Fürbeth, G. Grundmeier, R. Lösch and C. Reinartz, in: Corrosion mechanisms in Theory and Practice, Eds. P. Marcus, J. Oudar, Marcel Dekker, N. Y., 373 (1995).
28. E. Juzeliūnas, *Elektrokhimiya,* **28**, 1656 (1992).
29. A. Leng, Diploma thesis, University Düsseldorf (1991).
30. G. Sauerbrey, *Z. Phys.,* **155**, 206 (1959).
31. E. Juzeliūnas and M. Samulevičienė, *Electrochim. Acta,* **37**, 2611 (1992).
32. H.-H. Strehblow, in: Corrosion Mechnanisms in Theory and Practice, Eds. P. Marcus, J. Oudar, Marcel Dekker, N. Y., 201 (1995).

**K. Leinartas, M. Samulevičienė, A. Bagdonas, A. Sudavičius, E. Juzeliūnas**

**MAGNETRONINIO DULKINIMO BŪDU GAUTO FE–CR–NI–TA LYDINIO ELEKTROCHEMINIS IR KOROZINIS APIBŪDINIMAS**

S a n t r a u k a

Kvarco kristalo mikrogravimetrijos (KKM), elektrocheminio pilnutinės varžos spektroskopijos (EIS), pastoviosios srovės voltametrijos ir rentgeno fotoelektroninės spektroskopijos (RFS) metodais buvo tirta Fe–Cr–Ni–Ta lydinio, gauto magnetroniniu dulkinimo būdu (MD), korozinė ir elektrocheminė elgsena. MD dangų formavimui ant kvarco padėklų buvo naudojamas taikinys iš AISI 316 plieno ir gryno tantalo. Gautų lydinių elementinė sudėtis buvo nustatoma RFS metodu. Korozinė ir elektrocheminė MD dangų elgsena buvo tirta 5% NaCl (pH 5,75), 5% NaCl+HCl (pH 3,3) ir 10M HCl. Nustatyta, kad korozinis atsparumas Fe–Cr–Ni–Ta daug didesnis negu AISI 316 plieno. Tai parodė nulinės srovės potencialų, anodinių kreivių ir vadinamųjų „breakdown“ potencialų matavimų rezultatai. Tantalo inhibicinis efektas rūgščioje terpėje kur kas didesnis negu neutralioje. Nustatyta, kad Fe–Cr–Ni–Ta anodinis aktyvumas 5% NaCl yra apie 3 kartus mažesnis negu AISI 316, tuo tarpu 10M HCl šis skirtumas siekia apie 3 eilių reikšmes. KKM matavimais nustatyta, kad MD lydinys 10M HCl aktyviai koroduoja pradiniu imersijos momentu (~10 min), vėliau paviršius pasyvuojasi. RFS analizės duomenys parodė, kad korozijos metu susidariusioje pasyvioje plėvelėje gausu Ta, o tai ir sąlygoja korozijos inhibiciją.